Original Article





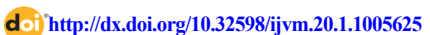
Morphological Evaluation and Osteometric Measurements of the Persian Cat's Antebrachium Bones Based on Computed Tomography Images

Hassan Nemati¹ 📵, Siamak Alizadeh^{2*} 📵, Mohammadreza Hosseinchi³ 📵

- 1. Faculty of Veterinary Medicine, Ur.C., Islamic Azad University, Urmia, Iran.
- 2. Department of Clinical Sciences, Nag.C., Islamic Azad University, Naghadeh, Iran.
- 3. Department of Basic Sciences, Ur.C., Islamic Azad University, Urmia, Iran.



How to Cite This Article Nemati, H., Alizadeh, S., & Hosseinchi, M. (2026). Morphological Evaluation and Osteometric Measurements of the Persian Cat's Antebrachium Bones Based on Computed Tomography Images. *Iranian Journal of Veterinary Medicine*, 20(1), 123-142. http://dx.doi.org/10.32598/ijvm.20.1.1005625



ABSTRACT

Background: Computed tomography (CT) is one of the most practical and accurate diagnostic imaging techniques to evaluate bones and joints in small animals.

Objectives: The present study aimed to investigate the morphology and osteometric measurements of the Persian cat's antebrachium bones based on CT images.

Methods: This cross-sectional descriptive study was conducted on 10 healthy adult Persian cats (5 males and 5 females). The anesthetized Persian cat was placed in a dorsoventral position on the CT scanner table with its forelimbs fully extended, and sagittal, transverse, and dorsal scans were performed from the proximal extremity of the metacarpals to the distal third of the humerus.

Results: Based on the study results, CT provides the possibility of identifying most of the anatomical structures of the forearm area of the Persian cat. In the CT images, the bones appeared white due to their high density, and their medullary cavities were dark. Additionally, muscles and tendons were visible on different gray scales. The structural details of the joint between the proximal extremity of the radius and the capitulum of the humerus and the joint between the distal extremity of the radius and the radial carpal bone could be better evaluated in the transverse CT plane. Proximal radioulnar and radiohumeral joints were examined better in transverse and sagittal CT plans. All details related to the olecranon, anconeal, and coronoid processes were visible in sagittal, transverse, and dorsal CT reconstructions. The structural features of the joint between the semilunar notch and trochlea of the humerus were more visible in the dorsal CT plane. Based on transverse CT images, the thickness of the cortex and the internal diameter of the medullary cavity of the radius and ulna bones were measured and statistically analyzed.

Conclusion: The results of this research indicate that the anatomical structures of the antebrachium bones of Persian cats are similar to those of other domestic cats. The study findings can be utilized in the teaching of computed tomographic anatomy, the interpretation of CT scan images, and performing clinical and treatment examinations of this breed of cat.

Keywords: Antebrachium bones, Computed tomography (CT), Morphologic, Osteometric, Persian cat

Article info:

Received: 14 Aug 2024 Accepted: 21 Oct 2024 Publish: 01 Jan 2026

* Corresponding Author:

Siamak Alizadeh, Associate Professor.

Address: Department of Clinical Sciences, Nag.C., Islamic Azad University, Naghadeh, Iran.

Phone: +98 (44) 33461731

E-mail: si.alizadeh@iau.ac.ir, S alizadeh01@yahoo.com



Copyright © 2026 The Author(s

Introduction

ne of the most famous cat breeds in the world is the Persian breed. The Persian cat or Iranian cat is a long-haired breed that has a round and flat face and a short muzzle. The age of this cat is about 10

years, but in good conditions, it may reach up to 19 years (Schmidt et al., 2022). The color of their eyes is blue or orange and is often blue in albino cats (Wilhelmy et al., 2016). The flat face type of the Persian cat, due to brachycephalic syndrome, has a round and large skull and a short nose. Feline antebrachii bones include two long bones: Radius and ulna, which are separate from each other and differentiated (Field & Taylor, 2018). The ulna bone is located on the caudal and medio-lateral surface of the radius. This bone is longer than the radius in cats. The proximal extremity of the ulna bone includes olecranon, anconeal, and coronoid processes (Reighard & Jennings, 2022). Bone morphometry is the study of quantitative and three-dimensional bone characteristics that are measured manually on bones or using diagnostic imaging techniques. The results of morphometric analyses in different animals can be used as a reference for evaluating the processes of bone, joint, and muscle diseases.

Computed tomography (CT) is one of the diagnostic imaging methods to investigate complications and diseases of bones and joints in exotic and small animals (Molazem et al., 2024; Keane et al., 2017; Atiyah & Alkattan, 2024). This non-invasive diagnostic imaging technique can display the structural features of the bones and joints of the body. Preston et al. (2015) performed radiography and CT scans of the forearms of dead cats. They described the characteristics of the bones in this area and declared their findings as a useful reference for future research and clinical applications. In this research, the average lengths of the radius and ulna were reported to be 95.89 and 114.67 mm, respectively, and the cancellous bone volume of the olecranon was 94.16 mm³. In a geometric accuracy study, Webster et al. (2019) investigated CT, micro-CT, and laser scanning methods for evaluating the articular surface of the distal radius in lost cats. They reported that articular surface models obtained from CT images exhibit dimensional errors, despite matching the voxel size. Based on this finding, they have stated that CT cannot be used for arthroplasty treatment decisions in small joints because it may not have the necessary accuracy to correct limb deformation or fracture repair. In another study, Major et al., described the CT findings of mycobacterial disease in infected cats and reported the skeletal complications caused by this disease, such as osteolytic and osteoproliferative lesions on the radius and ulna bones (Major et al., 2021). By researching cats suffering from elbow osteoarthritis, Ley et al. (2021) compared the diagnostic value of radiography and CT techniques, reporting that CT has more diagnostic value and can detect the early and mild stages of this disease. Rossi et al. (2003) investigated bilateral radioulnar synostosis with secondary elbow malformation in a sterile male cat by performing different diagnostic imaging methods. They claimed that CT is more diagnostic preferred compared to other diagnostic procedures. Assessment of the tomographic features of the Persian cat's antebrachium bones can be beneficial in identifying anatomical characteristics and pathological examinations. Different imaging techniques can be useful in diagnosing this type of damage. However, a precise examination of details related to the normal anatomy (morphology and morphometry) of these bones is necessary. Currently, radioanatomical studies of the forearm bones of the Persian cat are rare, and there are no detailed reports in this respect. Accordingly, this study aimed to investigate the morphology and osteometric measurements of the Persian cat's antebrachium bones by CT using 3D modeling. The results of this research can be used in identifying anatomical characteristics, investigating different species of Persian cats, teaching anatomical sciences and interpretation of CT scan images, as well as performing clinical and treatment examinations of this breed of cat.

Materials and Methods

Study design and animals

This cross-sectional descriptive study used 10 healthy adult Persian cats (5 males and 5 females) with an average age of 31.1 months and a mean weight of 4.9 kg, with proper nutrition (Table 1). The maturity of these cats was confirmed based on the plain radiographs (Catogram) obtained and the dental formula (Muhlbauer & Kneller, 2013; Gracis, 2018).

Anesthesia of cats

The cats used in the study were placed under general anesthesia using dissociative agents. For this purpose, a combination of medetomidine HCl (0.03-0.05 mg/kg, IM, Medetate® 0.1% injectable, Jorux, England), ketamine HCl (7-10 mg/kg, IM, Ketasol® 10% injectable, Alfasan, Holland), and butorphanol tartrate (0.4 mg/kg, Butomidor® 1% injectable, Richter Pharma, Austria) was applied through the intramuscular path (Corona et al., 2020).

Table 1. Weight and age of Persian cats

| Cata | | | N | /lale | | | | | Fe | male | | |
|-------------|-----|-----|-----|-------|-----|------|-----|-----|-----|------|-----|------|
| Cats | 1 | 2 | 3 | 4 | 5 | Mean | 1 | 2 | 3 | 4 | 5 | Mean |
| Weight (kg) | 4.8 | 5.5 | 6.2 | 5.8 | 5.3 | 5.5 | 3.7 | 4.2 | 4.8 | 4.5 | 4.4 | 4.3 |
| Age (m) | 24 | 30 | 27 | 36 | 42 | 31.8 | 21 | 26 | 40 | 35 | 30 | 30.4 |

CT studies

To prepare CT images, the anesthetized Persian cat was placed on the CT scan table in a sternal recumbent position, and its forelimbs were fully extended cranially. CT scans of the forearms were performed in the sagittal, transverse, and dorsal planes with a thickness of 1 mm and intervals of 2 mm from the proximal extremity of the metacarpals to the distal third of the humerus. A helical scanner (Toshiba multi-slice CT scanner Asteion Premium 4, Model: TSX-021B, Japan) was employed for CT. In addition, appropriate windows were selected to examine soft and bone tissues. The technical factors of the CT scanner included gantry rotation time (400 ms), slice thickness (1 mm), reconstruction distance (0.5–1 mm), pitch ratio (1), kVp (120), mAs (22), physical detector collimation (32×0.6 mm), final section collimation (64×0.6 mm), resolution (512×512 pixels), and resolution range (0.92×0.92), kernel (10 H), and increment (0.5 mm) (Ohlerth & Scharf, 2007; Badea, 2018). Imaging was performed based on the factors mentioned above, and the obtained images were saved in DICOM (Digital Imaging and Communications in Medicine) format (Brühschwein et al., 2018).

Three-dimensional reconstruction

Following saving the obtained images in DICOM format, they were transferred to a computer loaded with 3D modeling software (Onis CT software, Multi-Modality Workplace: VE 2.5A) (Wilhite & Wölfel, 2019). Next, these images were analyzed using bone (WW: 4000 HU; WL: 550 HU) and soft tissue (WW: 450 HU; WL: 80 HU) settings. The electronic caliper of this software was used for morphometric measurements.

Morphometric studies

The osteometric measurements of different parameters of the Persian cat's antebrachium bones and their means were recorded. Measurements were done once by the same person. The measured parameters and their descriptions are shown in Tables 2, 3, 4, 5, 6, 7, 8, 9 and 10. The NAV (Nomina Anatomica Veterinaria) was used

as the obtained scientific term (Veterinaria, 2017). The investigated parameters included (Preston et al., 2015; Webster et al., 2019; Özkadif et al., 2015):

Radius length (RL), ulna length (UL), olecranon tuberosity thickness (OTTh), olecranon cranio-caudal thickness (OCCTh), olecranon height (OH), humeral articular surface diameter in radius (HASDR), radius body diameter (RbD), ulna body diameter (UbD), ulna greater diameter in carpal articular surface (UGDCAS), ulna lesser diameter in carpal articular surface (ULDCAS), radius greater diameter in carpal articular surface (RGDCAS), and radius lesser diameter in carpal articular surface (RLDCAS) (Figure 1).

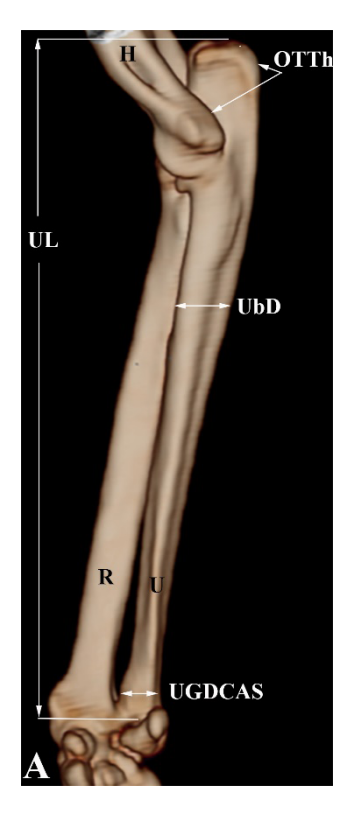
In the transverse CT reconstruction images, the inner diameter of the medullary cavity and the thickness of the cortex of the radius bone were measured at the levels of the radial head, radial neck, proximal third, middle part, and distal third, and radial trochlea. The settings (WW: 1600 HU and WL: 350 HU) and (WW: 900 HU and WL: 400 HU) were used to measure the medullary cavity and bone cortices, respectively (Figure 2).

Statistical analysis

The confidence interval (CI) index was used to calculate the normal size of the forearm bones and their component appendages in adult male and female Persian cats. Moreover, the parametric data were analyzed using an independent t test and the SPSS software, version 21. All variables were expressed as Mean \pm SD, and P \leq 0.05 is significant, with the confidence limit of 95%.

Results

Based on the study results, CT provides the possibility of identifying most of the anatomical structures of the forearm area of the Persian cat. In the CT images, the bones appeared white due to their high density, and their medullary cavities were dark. Additionally, muscles and tendons were visible on different gray scales. The structural details of the joint between the proximal extremity of the radius and the capitulum of the humerus, and



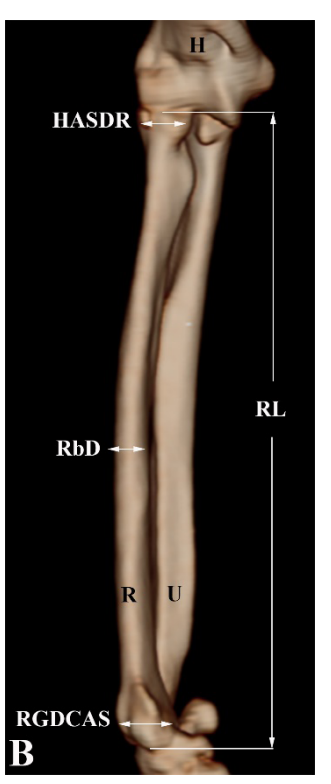


Figure 1. Parameters measured on 3D reformatted CT images in the lateromedial (A) and craniocaudal (B) levels of the right antebrachium bones of a 3-year-old male Persian cat

Abbreviations: RL: Radius length; UL: Ulna length; OTTh: Olecranon tuberosity thickness; HASDR: Humeral articular surface diameter in radius; RbD: Radius body diameter; UbD: Ulna body diameter; UGDCAS: Ulna greater diameter in carpal articular surface; and RGDCAS: Radius greater diameter in carpal articular surface.

the joint between the distal extremity of the radius and the radial carpal bone could be evaluated better in the transverse CT plane. Also, the proximal extremity of the radius was seen to be small in these images, but it was evident that it had a distinct neck and an expanded caput radii. Proximal radioulnar and radiohumeral joints were examined better in transverse and sagittal CT plans. All details related to the olecranon, anconeal, and coronoid processes were visible in sagittal, transverse, and dorsal CT reconstructions. The structural features of the joint between the semilunar notch and trochlea of the humerus were more visible in the dorsal CT plane. The styloid process of the distal extremity of the ulna bone could be examined in the sagittal and transverse planes. In this part, there was a convex facet that was in contact with the radius bone, which was only seen in the dorsal plan (Figure 3). Based on the measurements on the three-dimensional CT reconstruction images, the mean lengths of the radius and ulna in male Persian cats were 106.52±5.53 and 84.64±4.17 mm, respectively, and in females, 93.11±5.56 and 72.37±3.53 mm, respectively (95% confidence limits). Table 2 shows the external diameter of the radius and ulna in the measurement levels. The head of the radius appeared almost oval, and its average external diameter at the mediolateral surface was 37% of its craniocaudal surface. The neck of the radius was narrower than the head on both levels. The average lengths of the neck at the craniocaudal and mediolateral levels were respectively 84% and 80% of the radius head.

The external diameter of the diaphysis varied across different parts of the radius. The trochlea and radial head were the widest parts of the radius bone. The width of the radial trochlea was greater than the width of the radial head. The mean widths of the radial trochlea at the craniocaudal and mediolateral levels were 1.3 and 1.2 times the width of the radial head, respectively. The external diameter of the olecranon process at the craniocaudal level was approximately 64% of its mediolateral level. The external diameter of the olecranon process at the craniocaudal level was approximately 64% of its mediolateral level. The widest external part of the ulna was at the level of the coronoid process. The external diameter of the ulna at the craniocaudal level was more than at its mediolateral level. The external diameter of the ulna

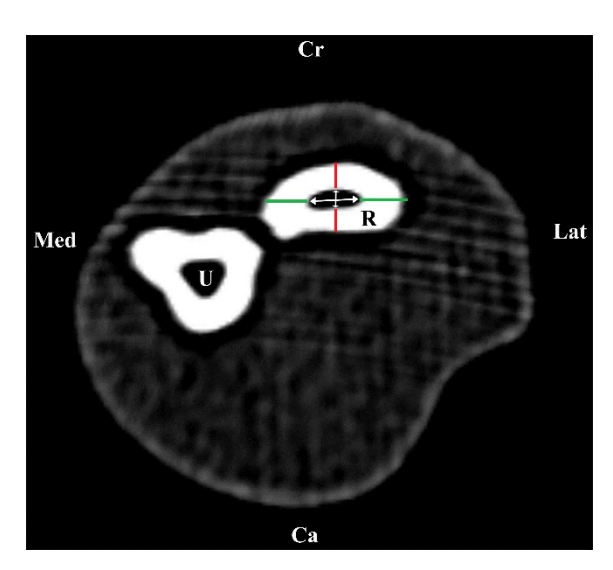


Figure 2. Measurement indices of the internal diameter of the medullary cavity and the thickness of the radius bone's cortex in the transverse CT image at the middle third level of the right forearm of a 3-year-old female Persian cat

Abbreviations: Cr: Cranial; Cd: Caudal; Med: Medial; Lat: Lateral; U: Ulna; R: Radius.

Note: Green lines: The thickness of the medial and lateral cortex; Red lines: The thickness of the cranial and caudal cortex; Big double arrow: The internal diameter of the medullary cavity at the mediolateral level; Small double arrow: The internal diameter of the medullary cavity at the craniocaudal level.

gradually decreased from the proximal to the distal side. Tables 3 to 6 show the thickness of the cortex of the radius and ulna bones at different levels. In all cats, the thickness of the caudal and medial cortex of the radial head was greater than its cranial and lateral cortex. The thickness of the cranial and caudal cortex of the radial neck was less than that of its lateral and lateral cortex. The thickness of the cranial and caudal cortex of the diaphysis and radial trochlea was less than that of its lateral and medial cortex. The thickness of the cranial, lateral, and medial cortexes of the olecranon process was equal, but the thickness of the caudal cortex was greater. The thickness of the caudal cortex of the olecranon process was more than 2 times that of the others. The thickness values of the cranial cortex of the coronoid process were 1.5, 4, and 1.4 times that of its caudal, medial, and lateral cortexes, respectively. The thickness of the caudal cortex of the ulnar diaphysis in the proximal third was more than in the other parts. In the middle part of the diaphysis of the ulna, the thickness values of the caudal cortex were approximately 2 times that of the lateral cortex, 1.6 times that of the cranial cortex, and 1.6 times that of the medial cortex. In the distal third of the ulna, the thickness values of the cranial cortex of the diaphysis were 1.3, 1.2, and 1.5 times that of the lateral, medial, and caudal cortex, respectively. Tables 7, 8, 9, and 10 show the internal diameter of the radius and ulna at different levels. The mean internal diameter of the radial head in the craniocaudal plane was 45% of its mediolateral plane. The medullary canal of the radius bone was almost oval. The

diameter of this canal in the middle third of the radius was narrower than its proximal and distal thirds. In the mediolateral plane, the average internal diameter values of the diaphysis of the radius in the proximal third were 1.15 and 1.07 times that of the middle part and the distal third, respectively. In the craniocaudal and mediolateral planes, the internal diameter of the radial trochlea was the widest part of the radius. In Persian cats, the caudal surface of the ulna was convex in the proximal third and the middle part, but gradually changed towards the distal side. The caudal surface of the ulna was completely concave in the distal third. In the craniocaudal plan, the olecranon process was the widest internal part of the ulna. In this plane, the internal diameter of the olecranon process was approximately 62% of its mediolateral plane. According to the transverse CT images, the diameter of the medullary canal of the olecranon process was narrower at the level of the coronoid process. The mean diameter values of the medullary canal of the olecranon process in the craniocaudal and mediolateral planes were 3.55 and 2.4 mm, respectively. In the craniocaudal plane, the average internal diameter of the ulna in the proximal third was 65% of its mediolateral plane. In the craniocaudal plane, the internal diameter of the ulnar diaphysis gradually decreased from proximal to distal. All parameters were reported in female cats, smaller than those of male cats. However, the parameters of ulna length, radius body diameter, and humeral articular surface diameter in radius were significantly smaller than those of male cats (P<0.05) (Table 2) (Figures 4 and 5).

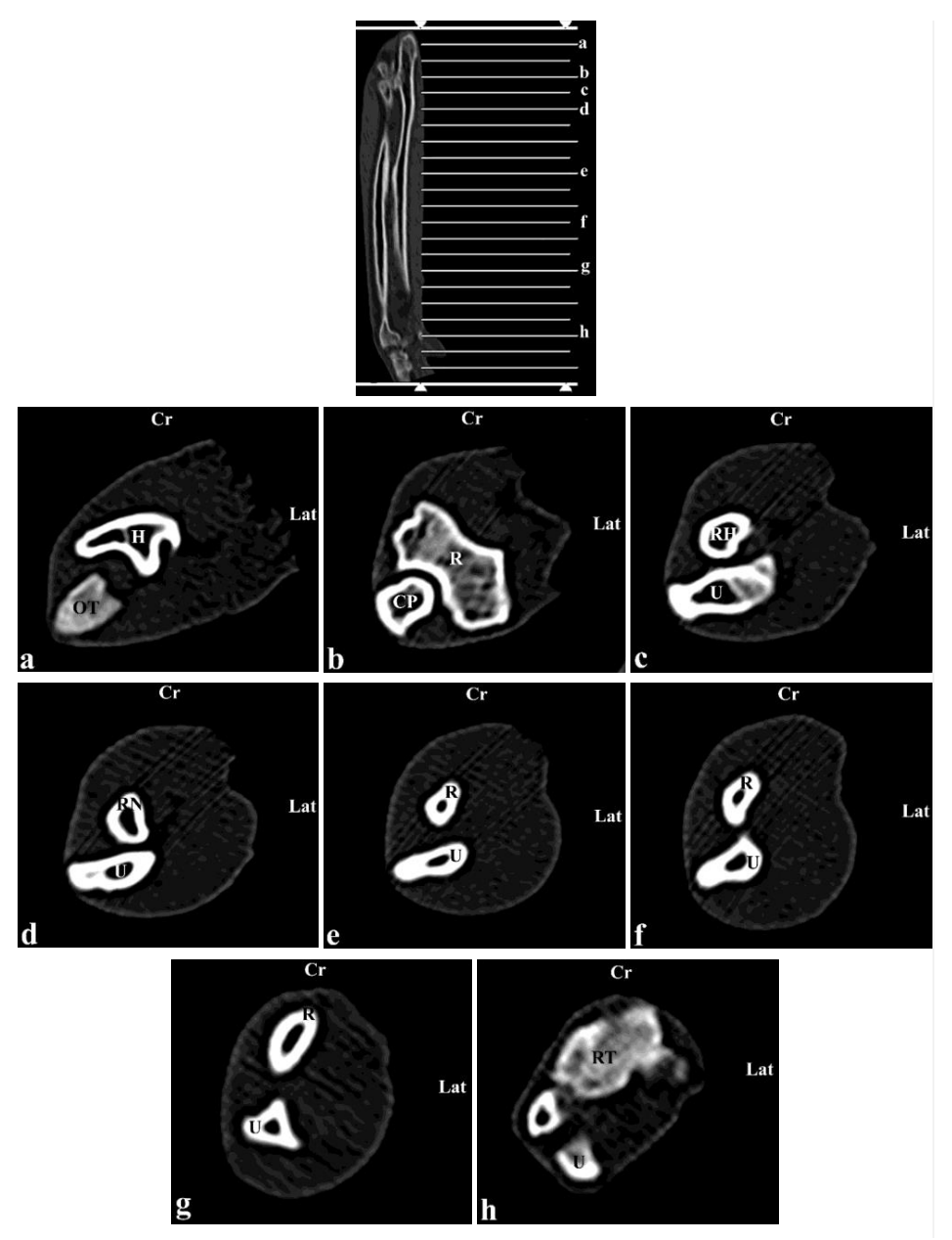


Figure 3. Transverse reformatted computed tomographic image of the right forearm of the same Persian cat in these levels: a) Olecranon tuberosity (OT), b) Coronoid process (CP), c) Radial head (RH), d) Radial neck (RN), e) Proximal third of the forearm, f) Middle third of the forearm, g) Distal third of the forearm, h) Radial trochlea (RT)

Abbreviations: R: Radius; H: Humerus; Cr: Cranial; Lat: Lateral; U: Ulna.

Discussion

Currently, various diagnostic imaging methods in pets are achievable and available. With the increase in the diagnostic standards of the veterinary profession, there is an increased demand for the use of advanced imaging methods (Farsijani & Safi, 2023; Zaidi et al., 2024). One of the most practical and accurate diagnostic imaging methods is the CT scan, which is especially used to evaluate the skeletal system of small animals (Da Costa

& Samii, 2010; Fidan et al., 2024). In recent years, reports have been published about the CT of cats, which were often related to the diagnosis of certain diseases (Garland et al., 2002; Onwuama et al., 2022). In all these cases, the presence of a normal CT scan image is necessary to determine the anatomical structures of the animal (Da Costa et al., 2020). However, there are few reports on the normal anatomy of domestic cats based on CT findings (Laborda-Vidal et al., 2022; Asgari & Pourhossein, 2024). In a study, Lewis et al. (2019) presented

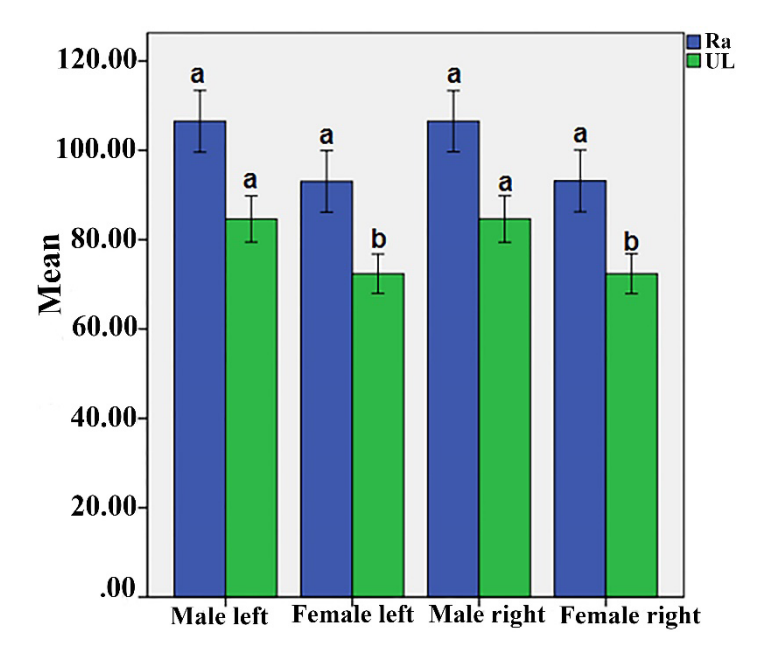


Figure 4. Values of left and right radius and ulna (mm) in male and female Persian cats

RbD: Radius body diameter; UbD: Ulna body diameter.

Note: The results were expressed as the Mean±SEM. Means within a column with different superscript letters (a-b) denote significant differences between male and female groups (P<0.05).

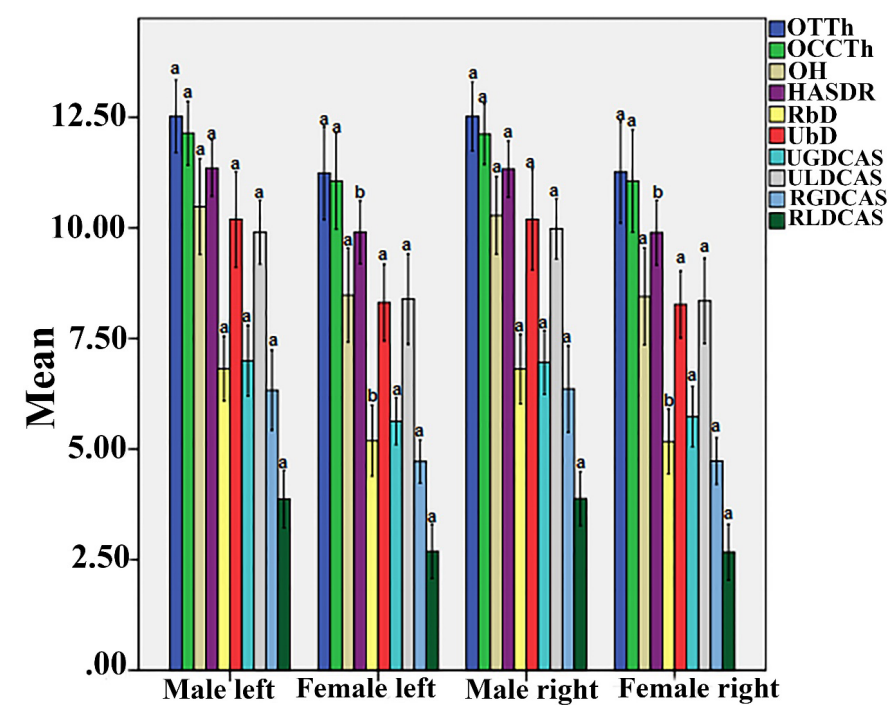


Figure 5. Values of left and right radius and ulna (mm) in male and female Persian cats

Abbreviations: OTTh: Olecranon tuberosity thickness; OCCTh: Olecranon cranio-caudal thickness; OH: Olecranon height; HASDR: Humeral articular surface diameter in radius; RbD: Radius body diameter; UbD: Ulna body diameter; UGDCAS: Ulna greater diameter in carpal articular surface; ULDCAS: Ulna lesser diameter in carpal articular surface; RGDCAS: Radius greater diameter in carpal articular surface; RLDCAS: Radius lesser diameter in carpal articular surface.

Note: The results were expressed as the Mean±SEM. Means within a column with different superscript letters (a-b) denote significant differences between male and female groups (P<0.05).

Table 2. Evaluation of radius and ulna variables (mm) in studied male and female Persian cats

| | | | Mean±SD | | |
|-----------|-------------------------|-------------------------|-------------------------|-------------------------|------------|
| Parameter | M | ale | Fen | nale | Total |
| | Right | Left | Right | Left | iotai |
| RL | 106.53±5.5° | 106.51±5.56ª | 93.17±5.57° | 93.06±5.55ª | 99.81±8.55 |
| UL | 84.65±4.19 ^a | 84.63±4.16 ^a | 72.37±3.59 ^b | 72.37±3.52 ^b | 78.5±7.23 |
| OTTh | 12.52±0.62° | 12.52±0.66ª | 11.26±0.92° | 11.24±0.85° | 11.88±0.96 |
| OCCTh | 12.12±.055ª | 12.14±0.58a | 11.06±0.93° | 11.06±0.88ª | 11.59±0.88 |
| ОН | 10.28±0.7 ^a | 10.48±0.87ª | 8.45±0.88 ^a | 8.48±0.85° | 9.42±1.24 |
| HASDR | 11.33±0.51 ^a | 11.35±0.51ª | 9.89±0.58 ^b | 9.9±0.57 ^b | 10.61±0.89 |
| RbD | 6.81±0.63ª | 6.82±.0.59ª | 5.17±0.59 ^b | 5.19±0.64 ^b | 5.99±1.01 |
| UbD | 10.19±0.91 ^a | 10.19±0.87ª | 8.27±0.61ª | 8.31±069ª | 9.24±1.21 |
| UGDCAS | 6.96±0.57ª | 7±0.64ª | 5.73±0.54° | 5.63±0.42° | 6.33±0.84 |
| ULDCAS | 9.98±0.54ª | 9.9±0.58ª | 8.35±0.77ª | 8.39±0.82° | 9.15±1.02 |
| RGDCAS | 6.36±0.78ª | 6.33±0.72 ^a | 4.73±0.42 ^a | 4.72±0.39 ^a | 5.53±1 |
| RLDCAS | 3.88±0.49 ^a | 3.87±0.52ª | 2.67±0.0.5ª | 2.69±0.49 ^a | 3.27±0.76 |

Abbreviations: RL: Radius length; UL: Ulna length; OTTh: Olecranon tuberosity thickness; OCCTh: Olecranon cranio-caudal thickness; OH: Olecranon height; HASDR: Humeral articular surface diameter in radius; RbD: Radius body diameter; UbD: Ulna body diameter; UGDCAS: Ulna greater diameter in carpal articular surface; ULDCAS: Ulna lesser diameter in carpal articular surface; RGDCAS: Radius greater diameter in carpal articular surface; RLD-CAS: Radius lesser diameter in carpal articular surface.

Note: $P \le 0.05$ is significant with the confidence limit of 95%. Different letters (a–b) denote significant differences between male and female groups (P < 0.05).

three-dimensional CT anatomy of the cat as a software program. In another study, Schuhegger (2021) described a comprehensive CT atlas of canine functional anatomy for the use of veterinary clinicians. In an anatomical study, Boonsri et al. (2019) reported no statistically significant difference between the osteometric sizes of the left and right limbs of a cat. In a similar study, Baranowski et al. (2012) stated no statistically significant difference between the left and right long bones of domestic cats. These studies are consistent with our research, and the results obtained in Persian cats are similar to those reported. Preston et al. (2015) examined the CT of the forearm bones of cats. They found that gender and age do not have a statistically significant effect on the crosssectional diameter of the bones. By performing biometric measurements of cat bones, Won et al. (2017) reported no statistically significant difference between males and females. These two recent studies are not consistent with our observations. According to this research, a statisti-

cally significant difference was observed between male and female Persian cats (Table 2).

CT anatomy can be used as a diagnostic reference and helps to evaluate breeds in some biometric research (Nguyen et al., 2013). In the present study, based on CT reconstruction images, various parameters of the Persian cat's forearm bones were evaluated and recorded. Most previous anatomical texts have only described the external anatomy of the forearm bones of the domestic cat. According to our investigations, no study has described the morphometry and morphology of the Persian cat's forearm using CT. In another study, Liblikas (2020) evaluated the effect of gonadectomy on the skeletal growth of domestic cats. They found no significant difference between males and females or the time of gonadectomy in the length of the radius. In addition, he has stated in this research that physeal closure is delayed in gonadectomized animals. In another study, Romero et al.

Table 3. The thickness (mm) of the left radial cortex at the determined levels based on transverse CT images in Persian cats

| | | | | Ma | le | | | | | Fe | emale | | |
|-------------------|-----|------|------|------|------|------|------|------|------|------|-------|------|------|
| Level | - | 1 | 2 | 3 | 4 | 5 | Mean | 6 | 7 | 8 | 9 | 10 | Mean |
| | Cr | 1.09 | 1.11 | 1.34 | 1.13 | 1.44 | 1.22 | 0.91 | 0.8 | 0.78 | 0.79 | 0.87 | 0.83 |
| Radial head | Cd | 1.39 | 1.45 | 1.33 | 1.45 | 1.55 | 1.43 | 1 | 1.09 | 1.14 | 1.2 | 1.07 | 1.1 |
| Radiai fiead | Med | 1.61 | 1.55 | 1.44 | 1.54 | 1.34 | 1.5 | 1.03 | 1.13 | 1.09 | 1.23 | 1.22 | 1.14 |
| | Lat | 0.92 | 0.87 | 0.67 | 0.78 | 0.67 | 0.78 | 0.69 | 0.79 | 0.78 | 0.54 | 0.45 | 0.65 |
| | Cr | 0.9 | 0.87 | 0.56 | 0.88 | 0.76 | 0.79 | 0.74 | 0.84 | 0.75 | 0.56 | 0.65 | 0.71 |
| Radial neck | Cd | 1.17 | 1.23 | 1.33 | 1.56 | 1.85 | 1.43 | 0.93 | 0.83 | 0.78 | 0.85 | 0.89 | 0.86 |
| Raulai Heck | Med | 1.78 | 1.78 | 1.45 | 1.34 | 1.45 | 1.56 | 1.45 | 1.35 | 1.35 | 1.35 | 1.54 | 1.41 |
| | Lat | 1.35 | 1.56 | 1.66 | 1.43 | 1.23 | 1.45 | 1.11 | 1.21 | 1.32 | 1.18 | 1.23 | 1.21 |
| | Cr | 1.45 | 1.34 | 1.45 | 1.56 | 1.76 | 1.51 | 1.14 | 1.24 | 1.33 | 1.16 | 1.42 | 1.26 |
| Proximal third | Cd | 1.8 | 1.78 | 1.77 | 1.78 | 1.87 | 1.8 | 0.61 | 0.71 | 0.65 | 0.47 | 0.23 | 0.53 |
| PIOXIIIIai tiliiu | Med | 2 | 2.11 | 2.34 | 2.09 | 2.03 | 2.11 | 1.6 | 1.5 | 1.45 | 1.88 | 1.76 | 1.64 |
| | Lat | 1.96 | 1.76 | 1.7 | 1.99 | 1.65 | 1.81 | 1.59 | 1.49 | 1.55 | 1.56 | 1.56 | 1.55 |
| | Cr | 1.34 | 1.78 | 1.65 | 1.43 | 1.35 | 1.51 | 1.15 | 1.25 | 1.43 | 1.32 | 1.45 | 1.32 |
| Middle | Cd | 1.22 | 1.45 | 1.56 | 1.45 | 1.22 | 1.38 | 0.96 | 0.86 | 0.79 | 0.76 | 0.87 | 0.85 |
| Midule | Med | 1.88 | 1.65 | 1.34 | 1.89 | 1.46 | 1.64 | 1.59 | 1.49 | 1.54 | 1.78 | 1.68 | 1.62 |
| | Lat | 1.69 | 1.34 | 1.67 | 1.88 | 1.76 | 1.67 | 1.41 | 1.41 | 1.33 | 1.48 | 1.54 | 1.43 |
| | Cr | 1.38 | 1.76 | 1.34 | 1.43 | 1.36 | 1.45 | 1.16 | 1.26 | 1.34 | 1.25 | 1.19 | 1.24 |
| Distal third | Cd | 1.18 | 1.87 | 1.78 | 1.23 | 1.34 | 1.48 | 1.08 | 1.18 | 1.22 | 1.11 | 1.08 | 1.13 |
| Distai tillia | Med | 1.76 | 1.67 | 1.77 | 1.67 | 1.56 | 1.69 | 1.44 | 1.34 | 1.21 | 1.35 | 1.46 | 1.36 |
| | Lat | 1.54 | 1.98 | 1.77 | 1.84 | 1.76 | 1.78 | 1.18 | 1.28 | 1.34 | 1.24 | 1.2 | 1.25 |
| | Cr | 0.94 | 0.88 | 0.56 | 0.56 | 0.45 | 0.68 | 0.66 | 0.76 | 0.67 | 0.56 | 0.65 | 0.66 |
| Radial trochlea | Cd | 0.94 | 0.87 | 0.65 | 0.65 | 0.6 | 0.74 | 0.66 | 0.56 | 0.64 | 0.54 | 0.56 | 0.59 |
| radiai trociilea | Med | 1.05 | 1.15 | 1.22 | 1.09 | 1.77 | 1.26 | 0.97 | 0.87 | 0.97 | 0.78 | 0.68 | 0.85 |
| | Lat | 1.08 | 1.15 | 1.1 | 1.06 | 1.14 | 1.11 | 0.83 | 0.69 | 0.85 | 0.81 | 0.67 | 0.77 |

Abbreviations: Cr: Cranial; Cd: Caudal; Med: Medial; Lat: Lateral.

(2022) reported that radius length was greater in gonadectomized cats compared to intact cats. All Persian cats used in our study were adults and had not been previously gonadectomized. Therefore, it is necessary to pay attention to this point when using the results of this study in clinical cases. It is suggested that the same parameters should be investigated in gonadectomized Persian cats in future studies, and the results should be compared with this study. Studies by Wells (2021) and Ocklenburg et al. (2019) show that cats have a preference for paws (same as right or left-handed persons), so the continuous preferential use of a limb may affect the quality and size of its bones. However, Stadig and Bergh (2015), by measuring the amount of pressure that each of the cat's limbs exerts on the ground, reported no significant difference between males and females in the preferential use of the

Table 4. The thickness (mm) of the right radial cortex at the determined levels based on the transverse CT images in Persian cats

| | | | | Mal | le | | | | | Fe | male | | |
|-------------------|-----|------|------|------|------|------|------|------|------|------|------|------|------|
| Level | - | 1 | 2 | 3 | 4 | 5 | Mean | 6 | 7 | 8 | 9 | 10 | Mean |
| | Cr | 1.19 | 1.32 | 1.23 | 1.29 | 1.22 | 1.25 | 0.81 | 0.79 | 0.59 | 0.56 | 0.67 | 0.68 |
| Radial head | Cd | 1.29 | 1.43 | 1.54 | 1.45 | 1.45 | 1.43 | 1.1 | 1.08 | 1.15 | 1.07 | 1.18 | 1.12 |
| Radiai fiead | Med | 1.51 | 1.54 | 1.34 | 1.43 | 1.46 | 1.46 | 1.13 | 1.09 | 1 | 1.11 | 1.15 | 1.1 |
| | Lat | 0.62 | 0.61 | 0.67 | 0.54 | 0.56 | 0.6 | 0.79 | 0.67 | 0.56 | 0.67 | 0.81 | 0.7 |
| | Cr | 0.8 | 0.68 | 0.76 | 0.61 | 0.4 | 0.65 | 0.84 | 0.79 | 0.62 | 0.77 | 0.67 | 0.74 |
| Radial neck | Cd | 1.27 | 1.93 | 1.85 | 1.81 | 1.32 | 1.64 | 0.83 | 0.74 | 0.59 | 0.78 | 0.78 | 0.74 |
| Naulai lieck | Med | 1.68 | 1.36 | 1.45 | 1.2 | 1.67 | 1.47 | 1.35 | 1.35 | 1.43 | 1.25 | 1.45 | 1.37 |
| | Lat | 1.45 | 1.26 | 1.23 | 1.35 | 1.42 | 1.34 | 1.21 | 1.31 | 1.33 | 1.43 | 1.32 | 1.32 |
| | Cr | 1.55 | 1.67 | 1.76 | 1.66 | 1.58 | 1.64 | 1.24 | 1.15 | 1.17 | 1.32 | 1.31 | 1.24 |
| Proximal third | Cd | 1.9 | 1.56 | 1.87 | 1.63 | 1.76 | 1.74 | 0.71 | 0.67 | 0.56 | 0.73 | 0.69 | 0.67 |
| Proximal tillu | Med | 2.1 | 2.09 | 2.03 | 2.11 | 2.16 | 2.1 | 1.5 | 1.39 | 1.55 | 1.65 | 1.64 | 1.55 |
| | Lat | 1.86 | 1.76 | 1.65 | 1.56 | 1.68 | 1.7 | 1.49 | 1.45 | 1.34 | 1.51 | 1.39 | 1.44 |
| | Cr | 1.24 | 1.45 | 1.35 | 1.45 | 1.32 | 1.36 | 1.25 | 1.19 | 1.2 | 1.28 | 1.33 | 1.25 |
| Middle | Cd | 1.32 | 1.34 | 1.22 | 1.43 | 1.31 | 1.32 | 0.86 | 0.67 | 0.56 | 0.91 | 0.77 | 0.75 |
| ivildale | Med | 1.68 | 1.43 | 1.46 | 1.31 | 1.68 | 1.51 | 1.49 | 1.39 | 1.54 | 1.51 | 1.49 | 1.48 |
| | Lat | 1.79 | 1.67 | 1.76 | 1.29 | 1.76 | 1.65 | 1.41 | 1.43 | 1.45 | 1.53 | 1.41 | 1.45 |
| | Cr | 1.68 | 1.45 | 1.36 | 1.46 | 1.45 | 1.48 | 1.26 | 1.29 | 1.33 | 1.29 | 1.26 | 1.29 |
| Distal third | Cd | 1.28 | 1.22 | 1.34 | 1.32 | 1.28 | 1.29 | 1.18 | 1.3 | 1.54 | 1.23 | 1.18 | 1.29 |
| Distai tilliu | Med | 1.86 | 1.54 | 1.56 | 1.49 | 1.56 | 1.6 | 1.34 | 1.25 | 1.65 | 1.37 | 1.34 | 1.39 |
| | Lat | 1.44 | 1.76 | 1.76 | 1.64 | 1.45 | 1.61 | 1.28 | 1.34 | 1.43 | 1.25 | 1.28 | 1.32 |
| | Cr | 0.84 | 0.45 | 0.45 | 0.53 | 0.78 | 0.61 | 0.76 | 0.61 | 0.45 | 0.76 | 0.68 | 0.65 |
| Radial trochlea | Cd | 0.84 | 0.6 | 0.56 | 0.52 | 0.67 | 0.64 | 0.56 | 0.54 | 0.51 | 0.62 | 0.66 | 0.58 |
| Nadiai ti Ocilied | Med | 1.15 | 1.25 | 1.24 | 1.31 | 1.15 | 1.22 | 0.87 | 0.78 | 0.64 | 0.78 | 0.78 | 0.77 |
| | Lat | 1.18 | 1.19 | 1.23 | 1.15 | 1.17 | 1.18 | 0.73 | 0.69 | 0.65 | 0.6 | 0.7 | 0.67 |

Abbreviations: Cr: Cranial; Cd: Caudal; Med: Medial; Lat: Lateral.

left or right limb. In another study, Xu et al. (2022) investigated the effect of gender on the use of the limbs of cats and found that the type of gender is not significant in the use of a specific limb. The results of our study are consistent with these reports.

Based on the results of the present study, no significant difference was observed in the left and right forearm parameters of a Persian cat. It seems that the reason is the low weight of Persian cats, and this weight is symmetrically distributed between the left and right sides. All parameters measured in the forearm bones of male Persian cats were more than those of females, the most important reason being the large size of male cats (Figure 6). The size of the parameters of the forearm bones is related to

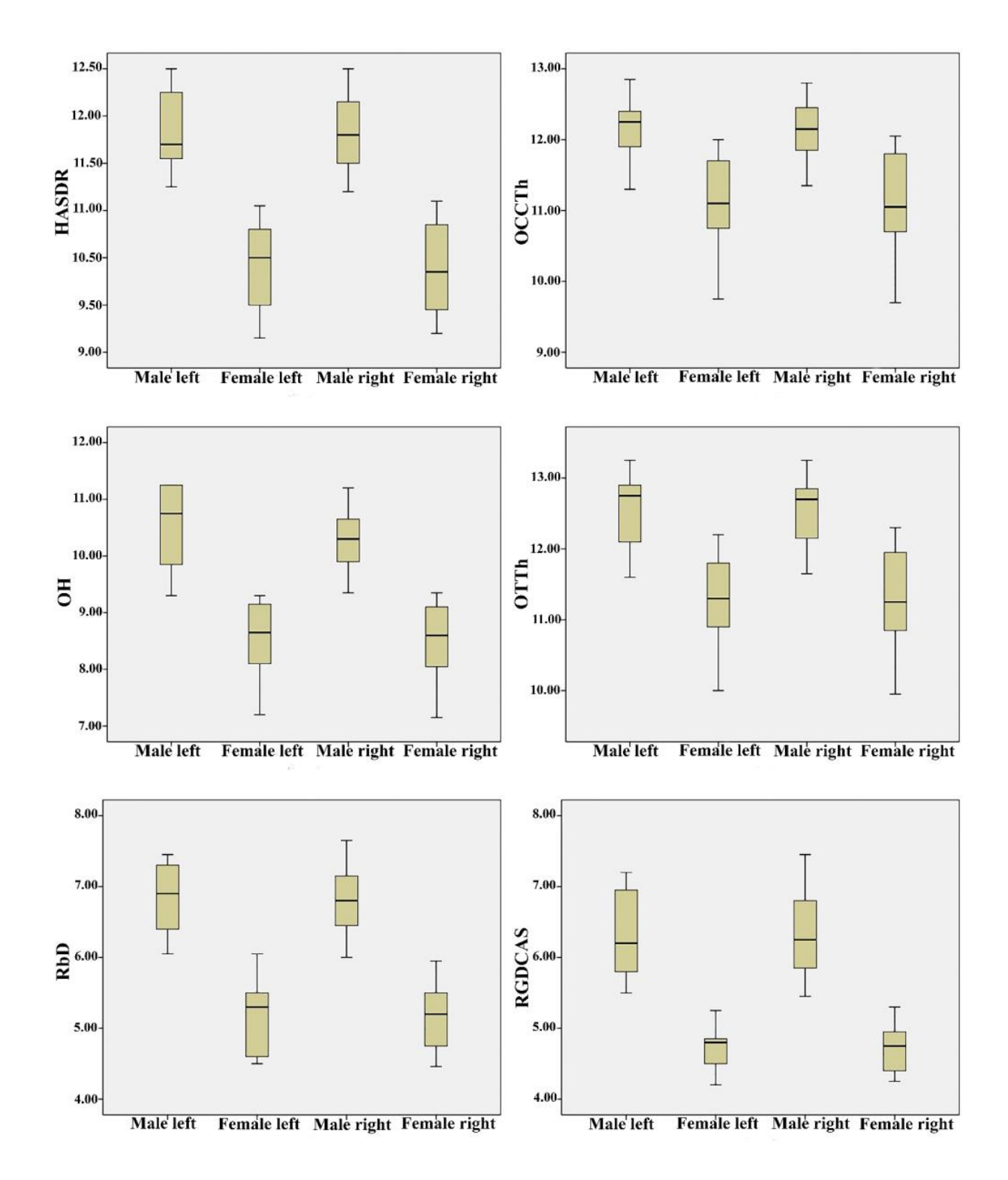
Table 5. The thickness (mm) of the left ulnar cortex at the determined levels based on the transverse CT images in Persian cats

| | | | | Mal | e | | | | | Fe | male | | |
|----------------------|-----|------|------|------|------|------|------|------|------|------|------|------|------|
| Level | | 1 | 2 | 3 | 4 | 5 | Mean | 6 | 7 | 8 | 9 | 10 | Mean |
| | Cr | 0.91 | 0.88 | 0.79 | 0.78 | 0.65 | 0.8 | 0.66 | 0.59 | 0.55 | 0.45 | 0.49 | 0.55 |
| Olecranon tuberosity | Cd | 1.98 | 1.78 | 1.9 | 1.87 | 1.67 | 1.84 | 1.41 | 1.39 | 1.43 | 1.39 | 1.43 | 1.41 |
| Olecianon tuberosity | Med | 0.87 | 0.88 | 0.68 | 0.67 | 0.65 | 0.75 | 0.59 | 0.65 | 0.54 | 0.48 | 0.45 | 0.54 |
| | Lat | 0.96 | 0.91 | 0.78 | 0.72 | 0.96 | 0.87 | 0.71 | 0.55 | 0.68 | 0.57 | 0.51 | 0.6 |
| | Cr | 5.06 | 5.1 | 5.01 | 5.09 | 5.06 | 5.06 | 4.39 | 4.44 | 4.43 | 4.33 | 4.43 | 4.4 |
| Coronoid process | Cd | 3.46 | 3.35 | 3.32 | 3.56 | 3.46 | 3.43 | 2.87 | 2.75 | 2.7 | 2.61 | 2.78 | 2.74 |
| coronola process | Med | 1.29 | 1.33 | 1.25 | 1.35 | 1.33 | 1.31 | 1.14 | 1.19 | 1.11 | 1.17 | 1.16 | 1.15 |
| | Lat | 3.91 | 3.87 | 3.78 | 3.79 | 3.91 | 3.85 | 3.25 | 3.33 | 3.2 | 3.19 | 3.15 | 3.22 |
| | Cr | 2.18 | 2.31 | 2.14 | 2.22 | 2.18 | 2.21 | 1.89 | 1.78 | 1.9 | 1.79 | 1.67 | 1.81 |
| Proximal third | Cd | 3.66 | 3.5 | 3.59 | 3.56 | 3.66 | 3.59 | 3.15 | 3.25 | 3.22 | 3.32 | 3.43 | 3.27 |
| Troximal tillid | Med | 1.39 | 1.38 | 1.41 | 1.45 | 1.41 | 1.41 | 1.07 | 1.1 | 1.03 | 1.03 | 1.07 | 1.06 |
| | Lat | 1.08 | 1.11 | 1.15 | 1.15 | 1.08 | 1.11 | 0.93 | 0.77 | 0.79 | 0.79 | 0.8 | 0.82 |
| | Cr | 1.38 | 1.29 | 1.27 | 1.45 | 1.38 | 1.35 | 1.14 | 1.19 | 1.11 | 1.14 | 1.11 | 1.14 |
| Middle | Cd | 2.61 | 2.65 | 2.57 | 2.56 | 2.61 | 2.6 | 1.86 | 1.87 | 1.56 | 1.65 | 1.56 | 1.7 |
| ivildule | Med | 1.42 | 1.39 | 1.43 | 1.54 | 1.56 | 1.47 | 1.22 | 1.2 | 1.31 | 1.29 | 1.24 | 1.25 |
| | Lat | 1.28 | 1.2 | 1.2 | 1.33 | 1.28 | 1.26 | 0.94 | 0.76 | 0.87 | 0.87 | 0.76 | 0.84 |
| | Cr | 1.62 | 1.56 | 1.67 | 1.59 | 1.62 | 1.61 | 1.35 | 1.39 | 1.41 | 1.54 | 1.61 | 1.46 |
| Distal third | Cd | 1.5 | 1.54 | 1.35 | 1.52 | 1.5 | 1.48 | 1.08 | 1.11 | 1.05 | 1.09 | 1.07 | 1.08 |
| Distai tiliiu | Med | 1.32 | 1.25 | 1.32 | 1.29 | 1.28 | 1.29 | 1.13 | 1.15 | 1.14 | 1.11 | 1.12 | 1.13 |
| | Lat | 1.13 | 1.09 | 1.11 | 1.17 | 1.1 | 1.12 | 0.97 | 0.88 | 0.85 | 0.78 | 0.75 | 0.85 |

Abbreviations: Cr: Cranial; Cd: Caudal; Med: Medial; Lat: Lateral.

the size and physical condition of the cat, and the influence of other factors, such as gender, handedness, and fertility status, is insignificant. In this study, the thickness of the slices was chosen to be 1 mm with an overlap of 0.5-0.75 mm to reduce the effects of partial average volume. The results of our study indicate that the distribution of the epiphysis is concentrated around the metaphyses of the radius and ulna, which was consistent with some reports of previous anatomical texts (Preston, 2015; Fox, 2021). The largest volume of epiphysis was in the distal radius and proximal ulna. According to our observations, about 15 mm of cancellous bone extended from the ulnar styloid process. The knowledge of this anatomical feature can allow the surgeon to place intramedullary pins in this

cancellous extremity of the ulna during surgery in this area. In some studies, it has been reported that the bone epiphyseal tissue can provide a high friction along with the high surface area of the bone-pin interface to prevent the risk of loosening and falling of the pin (Aithal et al., 2021). According to the findings of this research in Persian cats, the volume of the epiphysis in the radial head is smaller compared to the metaphysis portion. These observations were consistent with the anatomical studies of Brioschi et al. (2017) and Schellhorn and Sanmugaraja (2015). However, the radial neck in Persian cats was more prominent compared to other cat breeds, and was recognizable in the distal part of the proximal radioulnar, humeroulnar, and humeroradial joints.



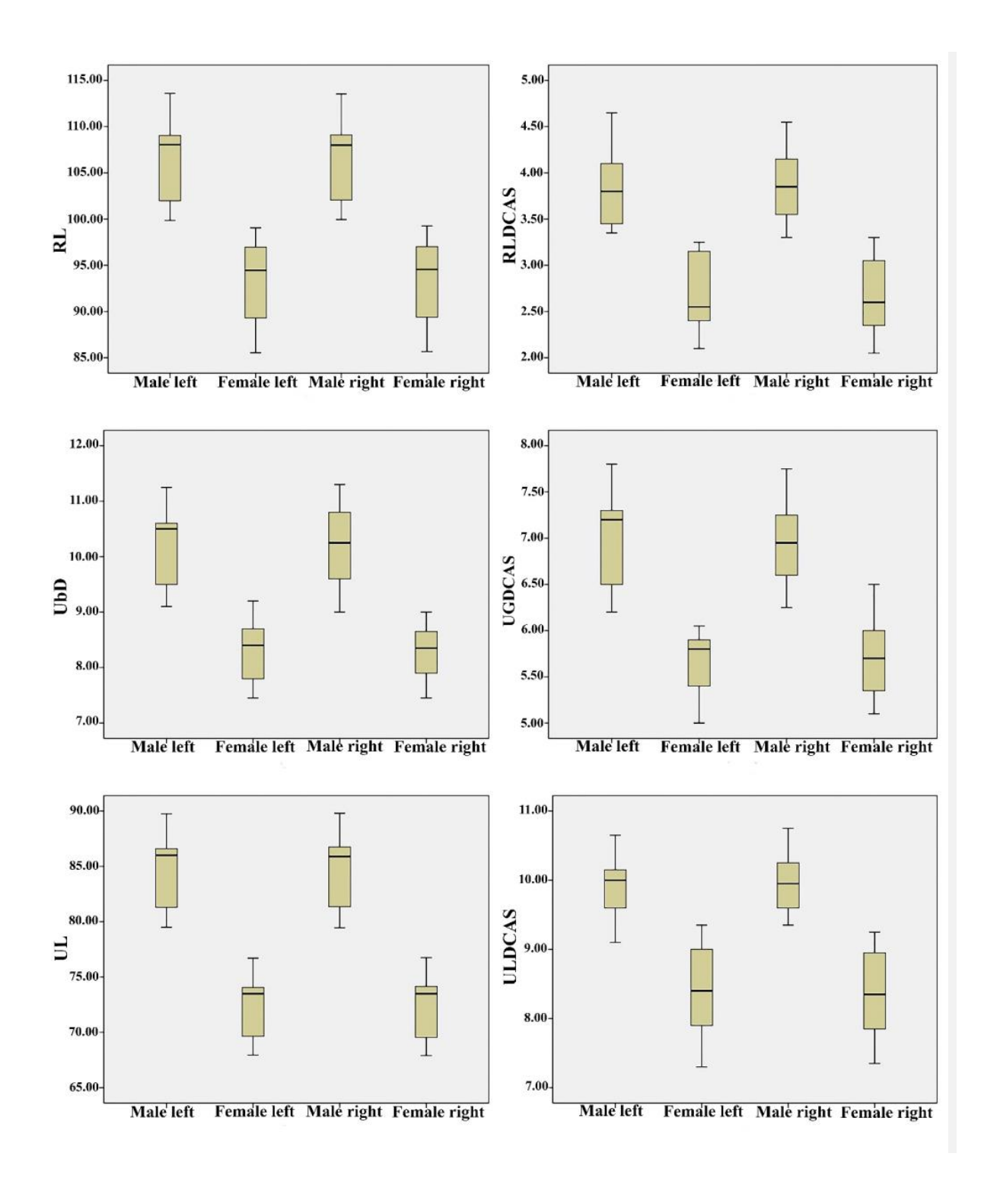


Figure 6. A box plot to compare RL, UL, OTTh, OCCTh, OH, HASDR, RbD, UbD, UGDCAS, ULDCAS, RGDCAS, and RLD-CAS factors of male and female Persian cats

Table 6. The thickness (mm) of the right ulnar cortex at the determined levels based on the transverse CT images in Persian cats

| | | | | Mal | le | | | | | Fei | male | | |
|----------------------|-----|------|------|------|------|------|------|------|------|------|------|------|------|
| Level | | 1 | 2 | 3 | 4 | 5 | Mean | 6 | 7 | 8 | 9 | 10 | Mean |
| | Cr | 0.81 | 0.79 | 0.8 | 0.69 | 0.77 | 0.77 | 0.76 | 0.66 | 0.69 | 0.81 | 0.69 | 0.72 |
| Olecranon tuberosity | Cd | 1.88 | 1.81 | 1.79 | 1.7 | 1.75 | 1.79 | 1.31 | 1.29 | 1.3 | 1.36 | 1.29 | 1.31 |
| Olecianon tuberosity | Med | 0.77 | 0.78 | 0.7 | 0.69 | 0.81 | 0.75 | 0.49 | 0.51 | 0.45 | 0.52 | 0.45 | 0.48 |
| | Lat | 0.86 | 0.77 | 0.78 | 0.91 | 0.69 | 0.8 | 0.81 | 0.78 | 0.78 | 0.87 | 0.85 | 0.82 |
| | Cr | 5.16 | 5.19 | 5.22 | 5.13 | 5.19 | 5.18 | 4.49 | 4.51 | 4.41 | 4.53 | 4.52 | 4.49 |
| Coronoid process | Cd | 3.56 | 3.45 | 3.35 | 3.67 | 3.64 | 3.53 | 2.97 | 2.88 | 2.88 | 2.9 | 2.77 | 2.88 |
| coronola process | Med | 1.39 | 1.43 | 1.44 | 1.45 | 1.42 | 1.43 | 1.24 | 1.33 | 1.23 | 1.34 | 1.19 | 1.27 |
| | Lat | 3.71 | 3.67 | 3.65 | 3.69 | 3.65 | 3.67 | 3.35 | 3.33 | 3.29 | 3.45 | 3.29 | 3.34 |
| | Cr | 2.78 | 2.71 | 2.59 | 2.66 | 2.69 | 2.69 | 1.69 | 1.75 | 1.78 | 1.75 | 1.87 | 1.77 |
| Proximal third | Cd | 3.56 | 3.6 | 3.63 | 3.63 | 3.61 | 3.61 | 3.25 | 3.33 | 3.33 | 3.25 | 3.31 | 3.29 |
| T TOXITION CHING | Med | 1.49 | 1.51 | 1.54 | 1.43 | 1.52 | 1.5 | 1.07 | 1.1 | 1.09 | 1.11 | 1.05 | 1.08 |
| | Lat | 1.18 | 1.22 | 1.15 | 1.2 | 1.23 | 1.2 | 0.93 | 0.88 | 0.78 | 0.95 | 0.83 | 0.87 |
| | Cr | 1.28 | 1.33 | 1.33 | 1.25 | 1.28 | 1.29 | 1.04 | 1.09 | 1.1 | 1.08 | 1 | 1.06 |
| Middle | Cd | 2.51 | 2.54 | 2.45 | 2.43 | 2.51 | 2.49 | 1.96 | 1.88 | 1.88 | 1.95 | 1.76 | 1.89 |
| Wildale | Med | 1.32 | 1.29 | 1.22 | 1.3 | 1.43 | 1.31 | 1.32 | 1.25 | 1.37 | 1.32 | 1.3 | 1.31 |
| | Lat | 1.38 | 1.41 | 1.32 | 1.38 | 1.35 | 1.37 | 0.84 | 0.76 | 0.76 | 0.78 | 0.7 | 0.77 |
| | Cr | 1.62 | 1.65 | 1.45 | 1.62 | 1.54 | 1.58 | 1.25 | 1.29 | 1.31 | 1.31 | 1.21 | 1.27 |
| Distal third | Cd | 1.4 | 1.36 | 1.31 | 1.4 | 1.45 | 1.38 | 1.18 | 1.15 | 1.15 | 1.22 | 1.15 | 1.17 |
| | Med | 1.42 | 1.45 | 1.39 | 1.39 | 1.51 | 1.43 | 1.13 | 1.15 | 1.17 | 1.15 | 1.11 | 1.14 |
| | Lat | 1.23 | 1.2 | 1.19 | 1.2 | 1.17 | 1.2 | 0.87 | 0.77 | 0.84 | 0.9 | 0.79 | 0.83 |

Abbreviations: Cr: Cranial; Cd: Caudal; Med: Medial; Lat: Lateral.

The thickness of the radial diaphysis cortex was almost uniform throughout its length. In contrast, the thickness of the ulna cortex varied in its different parts. The results of some studies show that the cortical thickness of the long bone diaphysis can change in its parts due to the influence of dynamic physiological loads. These factors can be caused by multiple pressures created on the subchondral bone or excessive stretching of tendons or ligaments at the connection to the bone diaphysis (Schultz & Wisner, 2011). In the present study, it was observed that the thickness of the cranial, medial, and lateral cortices of the olecranon process is similar. Still, the thickness of the caudal cortex was approximately 2.5 times that of the other parts. Since the tendon of the triceps muscle is

connected to the caudal cortex of this process, and this tendon is subjected to higher tensile forces, it may be the reason for the increase in the thickness of the cortex of this part. The thickness of the cranial cortex of the coronoid process was more than that of its other parts. The thickness of the cranial cortex of the coronoid process was 1.5, 4, and 1.4 times that of its caudal, medial, and lateral cortices, respectively. According to the findings of this study, the thickest cortex of the diaphysis of the ulna in Persian cats was related to its caudal part. The triangular section of the ulna bone is at this level and is the origin of the flexor digitorum profundus muscle tendon.

Table 7. The internal diameter (mm) of the right radial medullary cavity at the determined levels based on the transverse CT images in Persian cats

| Laval | | | | Ma | le | | | Female | | | | | | | |
|-----------------|---------|------|------|------|------|------|------|--------|------|------|------|------|------|--|--|
| Level | | 1 | 2 | 3 | 4 | 5 | Mean | 6 | 7 | 8 | 9 | 10 | Mean | | |
| Radial head | Cr-cd | 2.8 | 2.76 | 2.81 | 2.69 | 2.66 | 2.74 | 1.95 | 1.88 | 1.79 | 1.77 | 1.9 | 1.86 | | |
| Radiai fiead | Med-Lat | 6.19 | 6.22 | 6.25 | 6.15 | 6.32 | 6.23 | 4.07 | 4.09 | 4.1 | 4.09 | 4.04 | 4.08 | | |
| Radial neck | Cr-cd | 2.48 | 2.55 | 2.33 | 2.45 | 2.54 | 2.47 | 1.57 | 1.55 | 1.6 | 1.49 | 1.45 | 1.53 | | |
| Radiai fieck | Med-Lat | 3.81 | 3.78 | 3.76 | 3.7 | 3.7 | 3.75 | 2.31 | 2.45 | 2.3 | 2.39 | 2.29 | 2.35 | | |
| Proximal third | Cr-cd | 2.55 | 2.4 | 2.45 | 2.39 | 2.43 | 2.44 | 0.84 | 0.79 | 0.86 | 0.78 | 0.77 | 0.81 | | |
| Proximal third | Med-Lat | 3.28 | 3.33 | 3.33 | 3.3 | 3.37 | 3.32 | 1.71 | 1.69 | 1.8 | 1.65 | 1.71 | 1.71 | | |
| ۸۵:مامالم | Cr-cd | 2.09 | 2.12 | 2.05 | 2.15 | 2.16 | 2.11 | 1.07 | 1.05 | 1.09 | 1.06 | 1.07 | 1.07 | | |
| Middle | Med-Lat | 3.47 | 3.54 | 3.39 | 3.39 | 3.5 | 3.46 | 2.21 | 2.33 | 2.29 | 2.25 | 2.21 | 2.26 | | |
| Distal thind | Cr-cd | 2.38 | 2.45 | 2.33 | 2.36 | 2.48 | 2.4 | 1.26 | 1.29 | 1.31 | 1.3 | 1.32 | 1.3 | | |
| Distal third | Med-Lat | 3.66 | 3.51 | 3.56 | 3.45 | 3.51 | 3.54 | 2.57 | 2.66 | 2.5 | 2.65 | 2.6 | 2.6 | | |
| Dodiel trocklos | Cr-cd | 5.23 | 5.2 | 5.29 | 5.23 | 5.21 | 5.23 | 3.63 | 3.57 | 3.6 | 3.61 | 3.63 | 3.61 | | |
| Radial trochlea | Med-Lat | 7.5 | 7.3 | 7.35 | 7.41 | 7.55 | 7.42 | 7.25 | 7.2 | 7.2 | 7.29 | 7.22 | 7.23 | | |

Cr-Cd: Craniocaudal; Med-Lat: Mediolateral.

Table 8. The internal diameter (mm) of the left radial medullary cavity at the determined levels based on the transverse CT images in Persian cats

| Lovel | | | | Ma | le | | | Female | | | | | | |
|-----------------|---------|------|------|------|------|------|------|--------|------|------|------|------|------|--|
| Level | | 1 | 2 | 3 | 4 | 5 | Mean | 6 | 7 | 8 | 9 | 10 | Mean | |
| Radial head | Cr-cd | 2.5 | 2.55 | 2.45 | 2.49 | 2.52 | 1.86 | 1.88 | 1.86 | 1.77 | 1.69 | 1.8 | 1.8 | |
| Radiai fiead | Med-Lat | 6.29 | 6.33 | 6.19 | 6.31 | 6.32 | 4.08 | 4.07 | 4.06 | 4.1 | 4.09 | 4.07 | 4.08 | |
| Radial neck | Cr-cd | 2.38 | 2.41 | 2.3 | 2.35 | 2.34 | 1.53 | 1.61 | 1.65 | 1.61 | 1.59 | 1.61 | 1.61 | |
| Radiai fieck | Med-Lat | 3.75 | 3.7 | 3.56 | 3.65 | 3.71 | 2.35 | 2.22 | 2.2 | 2.21 | 2.22 | 2.25 | 2.22 | |
| Proximal third | Cr-cd | 2.35 | 2.34 | 2.45 | 2.32 | 2.32 | 0.81 | 0.76 | 0.68 | 0.76 | 0.76 | 0.76 | 0.74 | |
| Proximal unitu | Med-Lat | 3.4 | 3.35 | 3.38 | 3.35 | 3.44 | 1.71 | 1.66 | 1.56 | 1.55 | 1.66 | 1.66 | 1.62 | |
| Middle | Cr-cd | 2.22 | 2.29 | 2.2 | 2.2 | 2.25 | 1.07 | 1.07 | 1.09 | 1.07 | 1.07 | 1.07 | 1.07 | |
| Middle | Med-Lat | 3.53 | 3.55 | 3.56 | 3.45 | 3.55 | 2.26 | 2.35 | 2.31 | 2.35 | 2.35 | 2.31 | 2.33 | |
| Distal third | Cr-cd | 2.43 | 2.47 | 2.39 | 2.4 | 2.44 | 1.3 | 1.35 | 1.3 | 1.35 | 1.33 | 1.35 | 1.34 | |
| Distai tiliiu | Med-Lat | 3.55 | 3.5 | 3.45 | 3.51 | 3.56 | 2.6 | 2.66 | 2.56 | 2.66 | 2.66 | 2.66 | 2.64 | |
| Padial trachlos | Cr-cd | 5.45 | 5.47 | 5.34 | 5.42 | 5.5 | 3.61 | 3.74 | 3.69 | 3.74 | 3.75 | 3.69 | 3.72 | |
| Radial trochlea | Med-Lat | 7.6 | 7.55 | 7.59 | 7.56 | 7.61 | 7.23 | 7.11 | 7.15 | 7.09 | 7.14 | 7.12 | 7.12 | |

Cr-Cd: Craniocaudal; Med-Lat: Mediolateral.

Table 9. The internal diameter (mm) of the right ulnar medullary cavity at the determined levels based on the transverse CT images in Persian cats

| Level | | | | Ma | le | | | | | Fe | male | | |
|--------------------|---------|------|------|------|------|------|------|------|------|------|------|------|------|
| Level | | 1 | 2 | 3 | 4 | 5 | Mean | 6 | 7 | 8 | 9 | 10 | Mean |
| Olecranon tuberos- | Cr-cd | 7.25 | 7.19 | 7.21 | 7.33 | 7.31 | 7.26 | 6.31 | 6.33 | 6.29 | 6.34 | 6.25 | 6.3 |
| ity | Med-Lat | 3.21 | 3.19 | 3.22 | 3.25 | 3.27 | 3.23 | 2.2 | 2.22 | 2.2 | 2.2 | 2.19 | 2.2 |
| Coronoid process | Cr-cd | 3.75 | 3.69 | 3.77 | 3.7 | 3.75 | 3.73 | 2.57 | 2.55 | 2.56 | 2.55 | 2.57 | 2.56 |
| Coronola process | Med-Lat | 2.82 | 2.77 | 2.69 | 2.75 | 2.82 | 2.77 | 1.91 | 1.88 | 1.91 | 1.73 | 1.91 | 1.87 |
| Proximal third | Cr-cd | 4.18 | 4.22 | 4.19 | 4.33 | 4.25 | 4.23 | 2.06 | 2.09 | 2.06 | 2.07 | 2.06 | 2.07 |
| Proximal unitu | Med-Lat | 1.78 | 1.67 | 1.66 | 1.68 | 1.78 | 1.71 | 0.91 | 0.88 | 0.78 | 0.56 | 0.91 | 0.81 |
| Middle | Cr-cd | 3.14 | 3.19 | 3.16 | 3.13 | 3.15 | 3.15 | 2.17 | 2.22 | 2.17 | 2.17 | 2.17 | 2.18 |
| Middle | Med-Lat | 2.57 | 2.49 | 2.55 | 2.5 | 2.57 | 2.54 | 1.31 | 1.35 | 1.31 | 1.39 | 1.31 | 1.33 |
| Distal third | Cr-cd | 2.51 | 2.55 | 2.5 | 2.51 | 2.55 | 2.52 | 1.66 | 1.55 | 1.45 | 1.45 | 1.55 | 1.53 |
| Distal third | Med-Lat | 2.49 | 2.52 | 2.45 | 2.46 | 2.52 | 2.49 | 1.14 | 1.12 | 1.12 | 1.11 | 1.13 | 1.12 |

Cr-Cd: Craniocaudal; Med-Lat: Mediolateral.

The present study was a preliminary descriptive study on the morphometry and morphology of the Persian cat's antebrachium bones and had some limitations. The study results were based on research conducted in adult Persian cats and do not provide findings for immature or elderly cats. It is hoped that future studies will research immature Persian cats and other cat breeds, comparing more diverse groups. The results of this study can provide appropriate anatomical information for clinicians and surgeons to be used in clinical and orthopedic decisions of adult Persian cats.

Table 10. The internal diameter (mm) of the left ulnar medullary cavity at the determined levels based on the transverse CT images in Persian cats

| Lavel | | | | Mal | le | | | Female | | | | | | | |
|--------------------|---------|------|------|------|------|------|------|--------|------|------|------|------|------|--|--|
| Level | | 1 | 2 | 3 | 4 | 5 | Mean | 6 | 7 | 8 | 9 | 10 | Mean | | |
| Olecranon tuberos- | Cr-cd | 7.33 | 7.35 | 7.29 | 7.41 | 7.35 | 7.35 | 6.44 | 6.4 | 6.51 | 6.45 | 6.46 | 6.45 | | |
| ity | Med-Lat | 3.34 | 3.33 | 3.31 | 3.41 | 3.29 | 3.34 | 2.43 | 2.39 | 2.45 | 2.41 | 2.45 | 2.43 | | |
| Caranaid process | Cr-cd | 3.66 | 3.45 | 3.55 | 3.56 | 3.59 | 3.56 | 2.54 | 2.47 | 2.51 | 2.54 | 2.59 | 2.53 | | |
| Coronoid process | Med-Lat | 2.73 | 2.69 | 2.68 | 2.73 | 2.67 | 2.7 | 1.88 | 1.78 | 1.67 | 1.67 | 1.9 | 1.78 | | |
| Proximal third | Cr-cd | 4.33 | 4.25 | 4.25 | 4.34 | 4.27 | 4.29 | 2.11 | 2.17 | 2.12 | 2.11 | 2.15 | 2.13 | | |
| PIOXIIIIai tiiliu | Med-Lat | 1.56 | 1.5 | 1.45 | 1.53 | 1.54 | 1.52 | 0.88 | 0.69 | 0.78 | 0.76 | 0.78 | 0.78 | | |
| Middle | Cr-cd | 3.34 | 3.3 | 3.3 | 3.35 | 3.39 | 3.34 | 2.34 | 2.43 | 2.37 | 2.34 | 2.38 | 2.37 | | |
| ivildule | Med-Lat | 2.76 | 2.66 | 2.56 | 2.75 | 2.69 | 2.68 | 1.43 | 1.47 | 1.4 | 1.4 | 1.48 | 1.44 | | |
| Distal third | Cr-cd | 2.52 | 2.49 | 2.45 | 2.49 | 2.46 | 2.48 | 1.55 | 1.66 | 1.5 | 1.54 | 1.5 | 1.55 | | |
| Distal tillitu | Med-Lat | 2.55 | 2.44 | 2.5 | 2.51 | 2.51 | 2.5 | 1.22 | 1.29 | 1.22 | 1.23 | 1.21 | 1.23 | | |

Cr-Cd: Craniocaudal; Med-Lat: Mediolateral.

Conclusion

Based on the results of this study, CT is a useful diagnostic method to evaluate the skeletal system, especially assessing the forearm bones of Persian cats. Also, a specific examination of the tomographic characteristics of the antebrachium bones of this cat breed can be useful in evaluating their pathological disorders. In this study, the length, volume, surface area, cortex thickness, and internal and external diameter of the Persian cat's antebrachium bones were described, and their normal limits were determined. The results of this study indicate that the anatomical structures of the antebrachium bones of Persian cats are similar to those of other domestic cats. The findings of this study can be utilized in the teaching of computed tomographic anatomy, the interpretation of CT scan images, and performing clinical and treatment decisions for this cat breed.

Ethical Considerations

Compliance with ethical guidelines

This study was approved by the Faculty of Veterinary Medicine, Urmia Branch, Islamic Azad University, Urmia, Iran (Code: IR.IAU.URMIA.REC.1403.027) The procedures were carried out based on the guidelines of the Ethics Committee of the International Association for the Study of Pain. This work involved the use of methods that did not differ from established internationally recognized high standards (best practice) of veterinary clinical care for the individual animals.

Funding

This research did not receive any grant from funding agencies in the public, commercial, or non-profit sectors.

Authors' contributions

All authors contributed equally to the conception and design of the study, data collection and analysis, interception of the results and drafting of the manuscript. Each author approved the final version of the manuscript for submission.

Conflict of interest

The authors declared no conflict of interest.

Acknowledgments

The authors thank the Vice Chancellor for Research of Urmia Branch, Islamic Azad University, Urmia, Iran.

References

- Aithal, H. P., Pal, A., Kinjavdekar, P., & Pawde, A. M. (2023). Principles of fracture fixation techniques. In H. Prasad Aithal, A. Pal, P. Kinjavdekar, & A. M Pawde (Eds.). *Textbook of veterinary orthopaedic surgery* (pp. 65-153). New York: Springer. [DOI:10.1007/978-981-99-2575-9_2]
- Asgari, P., & Pourhossein, S. (2024). In vitro anti-Toxoplasma effects and apoptotic induction of queen bee acid (10-hydroxy-2-decenoic acid) alone and in combination with atovaquone. Archives of Razi Institute, 79(2), 321–326. [DOI:10.32592/ARI.2024.79.2.321] [PMID]
- Atiyah, A. G., & Alkattan, L. M. (2024). The role of fabricated coral shell powder in the healing of mandibular bone gap in dogs. *Iranian Journal of Veterinary Medicine*, 18(1), 489-500. [DOI:10.32598/ijvm.18.4.1005417]
- Badea, C. T. (2018). Small animal X-ray computed tomography. In P. Russo (Ed.), Handbook of X-ray imaging: Physics and technology (pp. 25), Boca Raton: CRC Press. [DOI:10.1201/9781351228251-36]
- Baranowski, P., Nowak, P., Pezinska, K., & Talaga, A. (2012). Osteometric traits of the selected skeleton elements of domestic cat (Felis silvestris F. catus) from archaeological sites Wolintown and Szczecin-vegetable market. Acta Scientiarum Polonorum. Zootechnica, 11(1), 3-23. [Link]
- Boonsri, B., Pitakarnnop, T., Buddhachat, K., Changtor, P., & Nganvongpanit, K. (2019). Can feline (Felis catus) flat and long bone morphometry predict sex or skull shape?. *Anatomical Science International*, 94(3), 245–256. [DOI:10.1007/s12565-019-00480-8] [PMID]
- Brioschi, V., Langley-Hobbs, S. J., Kerwin, S., Meeson, R., & Radke, H. (2017). Combined physeal fractures of the distal radius and ulna: Complications associated with K-wire fixation and long-term prognosis in six cats. *Journal of Feline Medicine and Surgery*, 19(8), 907–914. [DOI:10.1177/1098612X16653644] [PMID]
- Brühschwein, A., Klever, J., Wilkinson, T., Jr, & Meyer-Lindenberg, A. (2018). DICOM standard conformance in veterinary medicine in Germany: A survey of imaging studies in referral cases. *Journal of Digital Imaging*, 31(1), 13–18. [DOI:10.1007/s10278-017-9998-x] [PMID]
- Corona, D., Ranninger, E., Jörger, F., Goldinger, E., Stefan, A., & Torgerson, P. R., et al. (2020). Cats undergoing spay with medetomidine, ketamine and butorphanol develop arterial oxygen desaturation independent of surgical positioning and increased intraocular pressure in Trendelenburg position. Schweizer Archiv fur Tierheilkunde, 162(9), 539–550. [DOI:10.17236/sat00271] [PMID]
- da Costa, R. C., & Samii, V. F. (2010). Advanced imaging of the spine in small animals. *The Veterinary clinics of North America. Small Animal Practice*, 40(5), 765–790. [DOI:10.1016/j.cvsm.2010.05.002] [PMID]

- da Costa, R. C., De Decker, S., Lewis, M. J., Volk, H., & Canine Spinal Cord Injury Consortium (CANSORT-SCI) (2020). Diagnostic Imaging in Intervertebral Disc Disease. Frontiers in Veterinary Science, 7, 588338. [DOI:10.3389/fvets.2020.588338] [PMID]
- Farsijani, F., Safi, S., & Shirazi Beheshtiha, S. H. (2023). Comparison of the performance of bioresonance, electrophoresis and RT-PCR in the diagnosis of feline infectious peritonitis. Archives of Razi Institute, 78(3), 1077. [DOI:10.22092/ARI.2023.360790.2606] [PMID]
- Fidan, M. A., Özüdoğru, Z., & İlgün, R. (2024). Macro-anatomical Investigations on the Plexus Lumbosacralis of the Aksaray Malakli Dog. *Iranian Journal of Veterinary Medicine*, 18(1), 43-50. [DOI:10.32598/IJVM.18.1.10045433]
- Fox D. B. (2021). Physeal injuries and angular limb deformities. The Veterinary Clinics of North America. Small Animal Practice, 51(2), 305–322. [DOI:10.1016/j.cvsm.2020.11.003] [PMID]
- Garland, M. R., Lawler, L. P., Whitaker, B. R., Walker, I. D., Corl, F. M., & Fishman, E. K. (2002). Modern CT applications in veterinary medicine. *Radiographics*, 22(1), 55–62. [DOI:10.1148/radiographics.22.1.g02ja1155] [PMID]
- Gracis, M. (2018). Dental anatomy and physiology. In A. M. Reiter, & M. Gracis (Eds.), BSAVA manual of canine and feline dentistry and Oral surgery (pp.6-32). Quedgeley: BSAVA Library. [DOI:10.22233/9781905319602.2]
- Keane, M., Paul, E., Sturrock, C. J., Rauch, C., & Rutland, C. S. (2017). Computed tomography in veterinary medicine: Currently published and tomorrow's vision. In A. Mesrur Halefoglu (Ed.), Computed tomography-advanced applications (pp. 271-289). London: IntechOpen. [DOI:10.5772/66614] [PMID]
- Laborda-Vidal, P., Martín, M., Orts-Porcar, M., Vilalta, L., Melendez-Lazo, A., & de Carellán, A. G., et al. (2022). Computed tomography-guided fine needle biopsies of vertebral and paravertebral lesions in small animals. *Animals*, 12(13), 1688. [DOI:10.3390/ani12131688] [PMID]
- Lewis, T., Burnett, B., Tunstall, R., Abrahams, P., Nicholson, D., Chalk, C., & et al. (2019). Three-dimensional cat virtual anatomy: Development of an interactive virtual anatomical software. *Journal of Morphological Sciences*, 36(2), 105–114.
- Ley, C. J., Leijon, A., Uhlhorn, M., Marcelino, L., Hansson, K., & Ley, C. (2021). Computed tomography is superior to radiography for detection of feline elbow osteoarthritis. *Research in Veterinary Science*, 140, 6–17. [DOI:10.1016/j.rvsc.2021.07.025] [PMID]
- Liblikas, H. (2020). Prepubertal gonadectomy in male cats: a retrospective internet-based survey on the safety of castration at a young age [master's thesis]. Tartu: Estonian University of Life Sciences. [Link]
- Major, A., Holmes, A., Warren-Smith, C., Lalor, S., Littler, R., & Schwarz, T., et al. (2021). Computed tomographic findings in cats with mycobacterial infection. *Journal of Feline Medicine and Surgery*, 18(6), 510–517. [DOI:10.1177/1098612X15588799] [PMID]
- Molazem, M., Amini, E., Salimi, A., Muhammadnejad, A., & Hasannejad, H. (2024). Magnetic resonance imaging features of olfactory neuroendocrine carcinoma in a dog. *Iranian Journal of Veterinary Medicine*, 18(3), 447-452. [DOI:10.32598/ ijvm.18.3.1005276]

- Muhlbauer, M. C., & Kneller, S. K. (2024). *Radiography of the dog and cat: Guide to making and interpreting radiographs.* Hoboken: John Wiley & Sons. [DOI:10.1002/9781119564997]
- Nguyen, T. T. T., Szabó, C., & Nagy, I. (2013). Application of computer tomography in animal breeding: A review. *Állattenyésztés és Takarmányozás*, 62(2), 152-165. [Link]
- Ocklenburg, S., Isparta, S., Peterburs, J., & Papadatou-Pastou, M. (2019). Paw preferences in cats and dogs: Meta-analysis. *Laterality*, 24(6), 647–677. [DOI:10.1080/1357650X.2019.1578228] [PMID]
- Ohlerth, S., & Scharf, G. (2007). Computed tomography in small animals--basic principles and state of the art applications. *Veterinary Journal*, 173(2), 254–271. [DOI:10.1016/j.tvjl.2005.12.014] [PMID]
- Onwuama, K. T., Nzalak, J. O., Dzenda, T., Hambolu, J., & Salami, S. (2022). Onset and stages of osteogenesis in the rabbit (Oryctolagus cuniculus) using diaphonisation. *Iranian Journal of Veterinary Medicine*, 16(3), 228-238. [Link]
- Özkadif, S., Eken, E., Beşoluk, K., & Dayan, M. O. (2015). Threedimensional reconstruction of New Zealand rabbit antebrachium by multidetector computed tomography. *Iranian Jour*nal of Veterinary Research, 16(2), 205–209. [PMID]
- Preston, T. (2015). Biomechanical comparison of dual bone fixation in an ex-vivo mid-diaphyseal fracture model of the feline radius and ulna [doctoral dissertation]. Murdoch: Murdoch University. [Link]
- Preston, T., Glyde, M., Hosgood, G., & Snow, L. (2015). Morphometric description of the feline radius and ulna generated from computed tomography. *Journal of Feline Medicine and Surgery*, 17(12), 991–999. [DOI:10.1177/1098612X14564000] [PMID]
- Reighard, J., & Jennings, H. S. (2022). *Anatomy of the cat*. Maroussi: Alpha Edition. [Link]
- Romero, M. G., Marchetti, C., Priotto, M., Rodríguez, M., Gobello, C., & Furlan, P., et al. (2022). Evaluation of long-term effects of the gonadotrophin-releasing-hormone antagonist acyline on domestic-cat growth. *Topics in Companion Animal Medicine*, 50, 100680. [DOI:10.1016/j.tcam.2022.100680] [PMID]
- Rossi, F., Vignoli, M., Terragni, R., Pozzi, L., Impallomeni, C., & Magnani, M. (2003). Bilateral elbow malformation in a cat caused by radio-ulnar synostosis. *Veterinary Radiology & Ultrasound*, 44(3), 283–286. [DOI:10.1111/j.1740-8261.2003. tb00456.x] [PMID]
- Schellhorn, R., & Sanmugaraja, M. (2015). Habitat adaptations in the felid forearm. *Paläontologische Zeitschrift*, 89, 261-269. [DOI:10.1007/s12542-014-0230-8]
- Schmidt, M. J., Farke, D., Staszyk, C., Lang, A., Büttner, K., & Plendl, J., et al. (2022). Closure times of neurocranial sutures and synchondroses in Persian compared to Domestic Shorthair cats. *Scientific Reports*, 12(1), 573. [DOI:10.1038/s41598-022-04783-1] [PMID]
- Schuhegger, S. (2021). Body part regression for ct images. *arXiv*, 211-248 [Unpublished]. [Link]

- Schultz, R. M., & Wisner, E. R. (2011). Long bones. In T. Schwarz, & J. Saunders (Eds.), Veterinary computed tomography (pp. 381-386). Hoboken: Wiley Blackwell. [DOI:10.1002/9781118785676.ch37]
- Stadig, S. M., & Bergh, A. K. (2015). Gait and jump analysis in healthy cats using a pressure mat system. *Journal of Feline Medicine and Surgery*, 17(6), 523–529. [DOI:10.1177/1098612X14551588] [PMID]
- Veterinaria, N. A. (2017). International committee on veterinary gross anatomical nomenclature (ICVGAN). Hannover: Veterinaria.
- Webster, C. E., Marcellin-Little, D. J., Koballa, E. M., Stallrich, J. W., & Harrysson, O. L. A. (2019). Evaluation of the geometric accuracy of computed tomography and microcomputed tomography of the articular surface of the distal portion of the radius of cats. *American Journal of Veterinary Research*, 80(10), 976–984. [DOI:10.2460/ajvr.80.10.976] [PMID]
- Wells, D. L. (2021). Paw preference as a tool for assessing emotional functioning and welfare in dogs and cats: A review. *Applied Animal Behaviour Science*, 236, 105148. [DOI:10.1016/j. applanim.2020.105148]
- Wilhelmy, J., Serpell, J., Brown, D., & Siracusa, C. (2016). Behavioral associations with breed, coat type, and eye color in single-breed cats. *Journal of Veterinary Behavior*, 13, 80-87. [DOI:10.1016/j.jveb.2016.03.009]
- Wilhite, R., & Wölfel, I. (2019). 3D Printing for veterinary anatomy: An overview. *Anatomia, Histologia, Embryologia, 48*(6), 609–620. [DOI:10.1111/ahe.12502] [PMID]
- Won, S., Chung, W. J., & Yoon, J. (2017). Clinical application of quantitative computed tomography in osteogenesis imperfecta-suspected cat. *Journal of Veterinary Science*, 18(3), 415– 417. [DOI:10.4142/jvs.2017.18.3.415] [PMID]
- Xu, D., Zhou, H., Zhang, Q., Baker, J. S., Ugbolue, U. C., & Radak, Z., et al. (2022). A new method proposed to explore the feline's paw bones of contributing most to landing pattern recognition when landed under different constraints. Frontiers in Veterinary Science, 9, 1011357. [DOI:10.3389/fvets.2022.1011357] [PMID]
- Zaidi, S., Bessas, A., Hezil, D., Benseghir, H., & Bitam, I. (2024). Molecular surveillance of yersinia pestis from stray dogs and cats and their fleas in Algiers. *Archives of Razi Institute*, 79(2), 279–286. [DOI:10.32592/ARI.2024.79.2.279] [PMID]

